



Estimation of future climate change in cold weather areas with the LARS-WG model under CMIP5 scenarios

Jian Sha¹ · Xue Li¹ · Zhong-Liang Wang¹

Received: 18 April 2017 / Accepted: 15 January 2019 / Published online: 5 February 2019
© Springer-Verlag GmbH Austria, part of Springer Nature 2019

Abstract

Global warming has considerably challenged the natural environment and livelihood conditions. Understanding potential future changes in critical climatic variables, such as temperature and precipitation, is important for regional agricultural and water resource management. This study proposes a new approach to the application of the Long Ashton Research Station Weather Generator (LARS-WG) in Coupled Model Intercomparison Project Phase 5 (CMIP5) emission scenarios and aims to test its applicability in cold areas and to evaluate the response of temperature and precipitation, in amount and form, under future warmer climate trends. Three stations in northeastern China are set as case sites, and 50 years of daily weather observations are used for model calibration and validation. Future synthetic time-series of daily precipitation and daily maximum and minimum temperatures is generated by the calibrated LARS-WG based on three Representative Concentration Pathway (RCP) scenarios with various radiative forcing levels of 14 general circulation models (GCMs) outputs for the periods 2041–2060 (2050s) and 2061–2080 (2070s). The results show that the CMIP5 scenarios can be successfully used in a LARS-WG model and that the model performs well in cold weather conditions to repeat the current status of the case sites; the model is able to provide downscaling analysis for future daily weather generation via updating calibrated model parameters based on various GCM outputs. A generally warming and wetting conversion would last into the future for the study sites, but there is great inconsistency among different GCMs. An ensemble approach is adopted with mean values of multi-GCMs to avoid the uncertainty associated with using a single GCM, based on which the changes in the form of precipitation are further estimated. As a result of the decrease in freezing conditions, although annual precipitation will continue to increase in the future, there will be relatively less annual snowfall, which will be primarily focused in deep winter. Such changes in snow cover conditions will potentially disturb the original rules of local overwintering agriculture. In addition, more intense and earlier snowmelt discharge and more rainfall in summer will latently impact the watershed hydrologic process. The influences of climate change are significant, and related projects for agricultural and water resource management should be of great concern in local decision-making.

1 Introduction

Global climate change has placed great pressure on the world, and a consensus is building that global climate change will be a common challenge of humanity in the twenty-first century (McNutt 2013; Solow 2015). Climate change can alter the trends and timing of precipitation, temperature, and other

critical weather drivers; climate change can lead to a series of impacts on the environment and livelihood conditions, such as water resources, agriculture, and energy (Conway et al. 2015; Fezzi et al. 2015; Grafton et al. 2013). Many general circulation models (GCMs) have been created to address this issue (Sanchez et al. 2004; Stevens et al. 2013). Previous studies have estimated how the climate status might change in different areas and at different times under various possible emission scenarios (Gao et al. 2011; Giorgi and Lionello 2008). The results from GCMs, however, have insufficient spatial and temporal resolution and cannot be directly used in impact models to support specific local projects. Thus, it is desirable to explore a downscaling approach for GCM outputs, and many tools and methods have been proposed (Pervez and Henebry 2014; Tripathi et al. 2006). Stochastic weather generators, as one of the most typical and popular

Electronic supplementary material The online version of this article (<https://doi.org/10.1007/s00704-019-02781-4>) contains supplementary material, which is available to authorized users.

✉ Zhong-Liang Wang
wangzhongliang@vip.skleg.cn

¹ Tianjin Key Laboratory of Water Resources and Environment, Tianjin Normal University, Tianjin 300387, China

downscaling methods, have been widely applied for local scale weather simulation based on low-resolution GCM outputs (Vallam and Qin 2018; Wilby et al. 2002; Zhang 2005). At low cost and with less computationally demanding frameworks, it is simple to use weather generator models to quickly model future multiple-year weather data series at the daily time scale at a particular station. The Long Ashton Research Station Weather Generator (LARS-WG) is one of the most widely used weather generator models for climate change impact studies.

LARS-WG is a stochastic weather generator that was developed in 1997 for site synthetic weather time-series simulation (Semenov and Barrow 1997). LARS-WG uses a series of semi-empirical distributions to describe weather factors and calibrates and validates model parameters with long-time observed weather data records. LARS-WG has a great capability for maintaining consistency among the key statistical properties in synthetic and observed series and is able to repeat a site weather condition in the form of daily time-series for a suite of climate variables. By updating the model parameters based on the outputs of GCMs, LARS-WG can present the future weather characteristics in a site and generate a suite of synthetic daily climate variables, such as precipitation, maximum and minimum temperatures, and solar radiation. LARS-WG has been widely used to model weather events and estimate local climate change around the world. Chen et al. (2013) validated the applicability of the LARS-WG model in downscaling and predicting daily precipitation and daily maximum and daily minimum temperatures in Sudan and South Sudan to provide valuable information for the future planning and management of local water resources. Reddy et al. (2014) used a LARS-WG model to evaluate the change in climate over long periods in three semiarid areas in the southern Telangana region in India. Kumar et al. (2014) applied LARS-WG to estimate the impact of climate change on rainfall in Northwestern Bangladesh with multi-GCM ensembles. Sarkar et al. (2015) estimated further climate change in three arid locations of India by contrasting the baseline value with the downscaled output of LARS-WG based on seven GCMs. Ma et al. (2016) used LARS-WG to analyze precipitation and temperature changes in the historic period and future period in the Xiangjiang River Basin, China. Hassan et al. (2014) used LARS-WG to simulate and downscale rainfall and temperature and contrasted the model results with those of a Markov chain-based statistical downscaling model (SDSM). LARS-WG has been broadly applied, particularly in tropical and subtropical areas with few freezing conditions, for site and daily scale weather data generation and relevant analysis of the future climate status.

Furthermore, LARS-WG has also been widely used to estimate the impacts of climate change on agriculture and water resources through a model combination approach. Kim et al. (2013) used a combined LARS-WG and Soil and Water

Assessment Tool (SWAT) approach to assess the influence of climate change on crops and hydrological processes in the Yazoo River basin, Mississippi, USA. Bannayan et al. (2016) used LARS-WG to simulate future climate change and its impacts on maize production in northeastern Iran. Dumont et al. (2016) applied the LARS-WG model for a climatic uncertainty analysis in their work to assess and model the economic and environmental impacts of wheat nitrogen management in Belgium. Zarghami et al. (2011) applied LARS-WG to downscale precipitation and temperature and estimated the effects of climate change on runoffs using the artificial neural network (ANN) method in Iran. Mahat and Anderson (2013) used a combination of LARS-WG and a conceptual hydrological model, HBV-EC, to evaluate the impacts of climate and forest changes on streamflow together with GLUE uncertainty analysis in Southern Alberta, Canada. Qin and Lu (2014) used a linkage of the LARS-WG model and a hydrological model to estimate the flood risk of the Heshui watershed in southern China. Previous applications have shown the great ability of LARS-WG to analyze and predict the changes in critical climatic variables and provide valuable reference results for the future planning and management of agricultural and/or water resources worldwide.

However, the scenario analysis module in the latest version of LARS-WG was developed based on the old SRES emissions scenario from the IPCC Fourth Assessment Report (AR4), which limited its scope and value for application. The new Coupled Model Intercomparison Project Phase 5 (CMIP5) emission scenarios in IPCC AR5 have been widely used for future climate status estimations, and the integrated application of LARS-WG with AR5 scenarios was a great concern in recent studies (Ahmadzadeh Araj et al. 2018; Fenta Mekonnen and Disse 2018; Semenov and Stratonovitch 2015). Previous studies have indicated that it is critical to perform valid LARS-WG applications using a suitable approach to update the LARS-WG parameters based on the outputs of GCMs under AR5 scenarios; there is a great demand to bridge this gap between LARS-WG and GCMs for developing various approaches, which are still insufficient and must be complemented. In this study, we proposed a relatively convenient approach based on the public climate data of gridded GCM outputs in WorldClim (Hijmans et al. 2005) and a batch command of ArcGIS 10.2 in Python, which was able to achieve site-scale climate change estimations available for LARS-WG application. In addition, while it has mainly been used in tropical and subtropical areas, the LARS-WG was applied to three weather stations in northeastern China to test the model's applicability in temperate areas with cold weather conditions in winter. The changes in air temperature and precipitation behavior were estimated for two future periods of 2041–2060 (2050s) and 2061–2080 (2070s). The integrated effects on snow, snowmelt, and rain due to a rise in

temperature and changes of precipitation (in amount and intensity) are of great concern. Detailed model applications and a discussion of the results are described below.

2 Materials and methods

2.1 Study area and data description

The northern-most three weather stations, namely Huma, Nenjiang, and Sunwu, in northeastern China, were selected as case sites for the study (Fig. 1). These sites are located in the Heilongjiang watershed and were characterized under cold weather conditions. The latitude, longitude, and altitude of Huma, Nenjiang, and Sunwu are 51.72° N, 126.65° E, 177.40 m; 49.17° N, 125.23° E, 242.20 m; and 49.43° N, 127.35° E, 234.50 m, respectively. The mean temperatures of the base period (1961–2010) at Huma, Nenjiang, and Sunwu were −0.56 °C, 0.62 °C, and −0.21 °C, respectively, and were only −22.96 °C, −21.30 °C, and −21.26 °C in winter (December, January, and February). The average annual rainfall of the base period at these three sites was 465 mm, 476 mm, and 540 mm, respectively.

A historical baseline of weather data from 1961 to 2010 (50 years) was used for LARS-WG calibration to determine the model parameters. The weather data indexes included the daily minimum temperature, daily maximum temperature,

daily precipitation, and sunshine hours. All data for the observed weather records were downloaded from the China Meteorological Data Service Center (CMDC).

2.2 LARS-WG model approach

The newest version of LARS-WG 5 was used in this study. As a stochastic weather generator, LARS-WG 5 can simulate the daily weather factors for any length of time based on a series of semi-empirical distribution frameworks. LARS-WG utilizes histograms with 23 intervals to describe the distribution of the lengths of wet and dry day series, daily precipitation, and daily maximum (Tmax) and minimum temperatures (Tmin). Synthetic weather data are generated as random values from relevant semi-empirical distributions, which were chosen by first selecting one interval and then selecting a value within that interval from the uniform distribution. The interval bounds and proportion of events in each interval are the model parameters that must be calibrated based on historical data. In this study, we first used 50 years of observed daily weather data for model calibration to determine the model parameters, based on which 50 years of synthetic daily weather data were generated for model validation. Independent parameter sets were calibrated for each site, and the groups of observed and synthetic daily weather data were compared using statistical tests and graphical comparisons to test the validity of the model. Then, using the calibrated LARS-WG

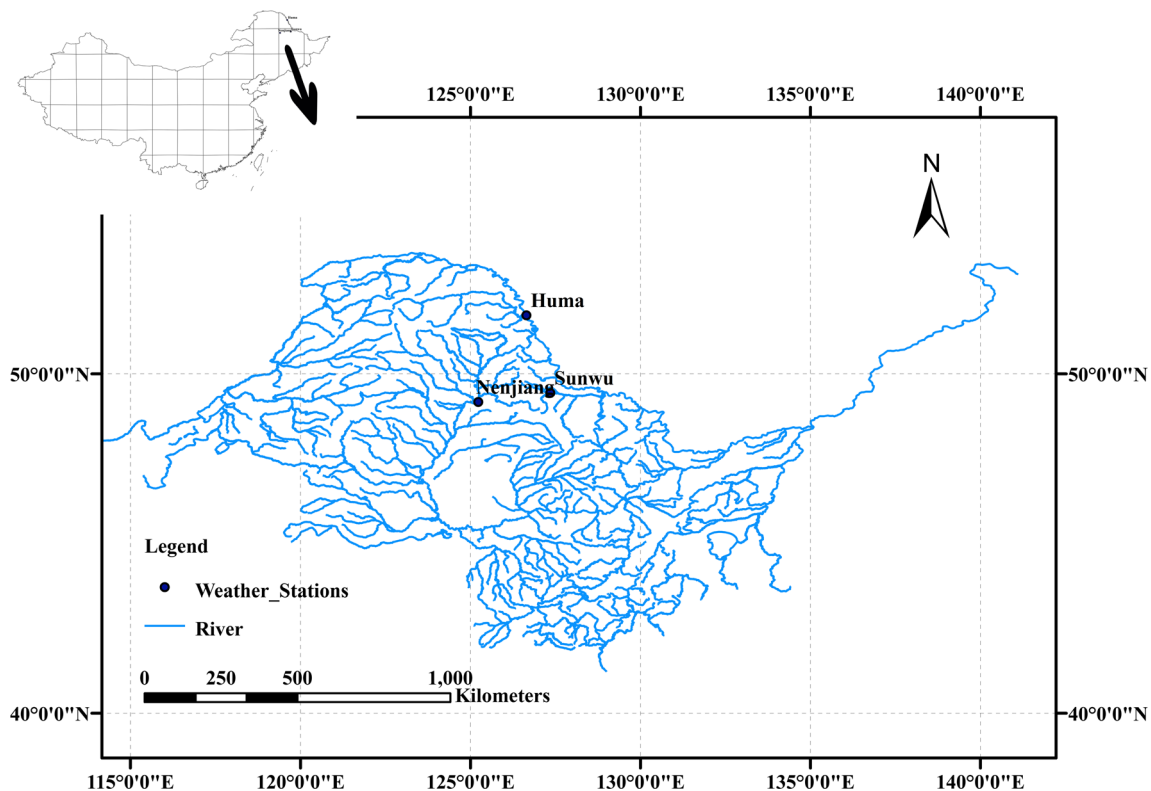


Fig. 1 Location of the weather stations in this study

model, future weather data series were generated by updating the model parameters based on different climate scenarios from different GCMs outputs.

The GCM outputs used for updating the LARS-WG parameter were estimated based on the global gridded maps from the WorldClim version 1.4 dataset, which provided average monthly climate data layers for minimum and maximum temperatures and precipitation for current conditions and future conditions from downscaled GCMs data based on CMIP5 scenarios. Three Representative Concentration Pathway (RCP) scenarios that represented different radiative forcing levels were used in this paper, including RCP 2.6, RCP4.5, and RCP8.5. Fourteen different GCM outputs for each RCP scenarios in two future periods, 2046 to 2065 (2050s) and 2060 to 2079 (2070s), were considered, including BCC-CSM1-1, CCSM4, CNRM-CM5, GFDL-CM3, GISS-E2-R, HadGEM2-AO, HadGEM2-ES, IPSL-CM5A-LR, MIROC-ESM-CHEM, MIROC-ESM, MIROC5, MPI-ESM-LR, MRI-CGCM3, and NorESM1-M. For each GCM, there is a series of gridded maps that represent the global average monthly values for one weather factor in one future period under one RCP scenario. The “Extract Value to Points” function in Spatial Analyst Tools in ArcGIS 10.2 was used to obtain the grid values for the three points of the case sites in this study, and a Python batch command was developed (provided in the [Supplemental Material](#)) to collect and summarize monthly weather data for all GCM result maps. Then, changes in the monthly Tmax, Tmin, and precipitation were calculated and used to update the LARS-WG parameters for each scenario and period, based on which groups of 50-year synthetic daily weather data were generated for further discussions of climate change properties.

3 Results and discussion

3.1 Modeling performance

Three general statistical tests were performed on various weather items to assess the performance of the LARS-WG model. First, the Kolmogorov–Smirnov (K–S) test was performed to compare the consistency of the observed series and synthetic series on four items, including seasonal wet/dry series distributions (WDSeries), daily precipitation distributions (PrecD), daily minimum temperature distributions (TminD), and daily maximum temperature distributions (TmaxD). Second, the *t* test was performed to determine whether the observed and synthetic series significantly differed from each other on three items, namely the monthly mean of precipitation (PMM), monthly mean of daily maximum temperature (TmaxM), and monthly mean of daily minimum temperature (TminM). Additionally, the monthly variances of precipitation

(PMV) of the observed and synthetic series were estimated via the *F*-test. A summary of test results is provided in Table 1 with a series of numerals that indicate the numbers of tests, revealing significantly different results at the 5% significance level out of the total number of tests. The larger the number is, the poorer the model performance is. Otherwise, with a small number of significantly different results, the model performance could be classified as excellent with reliable outputs, which occurred in this instance. None of the WDSeries, PrecD, TminD, TminM, and TmaxD at all three sites had significantly different results; for PMM, PMV, and TmaxM, the average numbers with significant results were 0.67, 1.33, and 0.33, respectively, out of 12 tests for each site. These results indicated excellent modeling precision for LARS-WG used in northeast China, and the LARS-WG model can better simulate the daily temperature and rainfall distributions in comparison to the monthly means and variance, but all of the results were acceptable (Amin et al. 2014; Naderi and Raeisi 2016).

Additionally, the simulated and observed mean monthly precipitation and standard deviation, as well as the monthly mean of the daily maximum and minimum temperatures, were compared and visualized with a series of graphical comparisons in Figs. 2 and 3. On the one hand, the mean monthly precipitation between the simulated and observed series show great consistency, and the errors mainly occur in the summer months with high precipitation (Fig. 2a1–a3). Similarly, the discrepancies in the standard deviation of monthly precipitation focus on high precipitation months, while the overall performance is also poorer than that of the mean estimation (Fig. 2b1–b3). Finding a perfect simulation for the standard deviation is a common issue among statistical downscaling models. For the precipitation simulation, it requires a combination of several estimations. We must estimate whether a day is a wet day (with precipitation > 0), and if so, we must estimate how much precipitation occurs. Furthermore, because this study uses a semi-empirical interval approach for estimating the precipitation yield in LARS-WG instead of a probability distribution directly based on observed means and standard deviations in other weather generators, there is more potential uncertainty in the variability of monthly precipitation. Furthermore, due to the use of the wet/dry series approach rather than of Markov chains in LARS-WG, there is some additional uncertainty at the beginning and end of months when we compile the results based on individual months. The linkage of various uncertainties will ultimately be reflected in the monthly precipitation estimations so that the simulated results will have discrepancies in mean and standard deviation, particularly in summer months due to abundant rain. The test statistics, however, show that no significant difference for most months between the simulated and observed series, and the model results for the precipitation

Table 1 Results of the statistical tests comparing the observed data and synthetic data generated by LARS-WG with the numbers of tests revealing significant different results at the 5% significance level

Sites	WDSeries ^a	PrecD ^b	PMM ^c	PMV ^d	TminD ^e	TminM ^f	TmaxD ^g	TmaxM ^h
Huma	0	0	1	0	0	0	0	1
Nenjiang	0	0	1	2	0	0	0	0
Sunwu	0	0	0	2	0	0	0	0
Average	0	0	0.67	1.33	0	0	0	0.33
Total tests	8	12	12	12	12	12	12	12

^a Seasonal wet/dry series distributions tested by the Kolmogorov–Smirnov (K–S) test

^b Daily precipitation distributions tested by the Kolmogorov–Smirnov (K–S) test

^c Monthly mean of precipitation tested by the t-test

^d Monthly variances of precipitation tested by the F-test

^e Daily minimum temperature distributions tested by the Kolmogorov–Smirnov (K–S) test

^f Monthly mean of daily minimum temperature tested by the t-test

^g Daily maximum temperature distributions tested by the Kolmogorov–Smirnov (K–S) test

^h Monthly mean of daily maximum temperature tested by the t-test

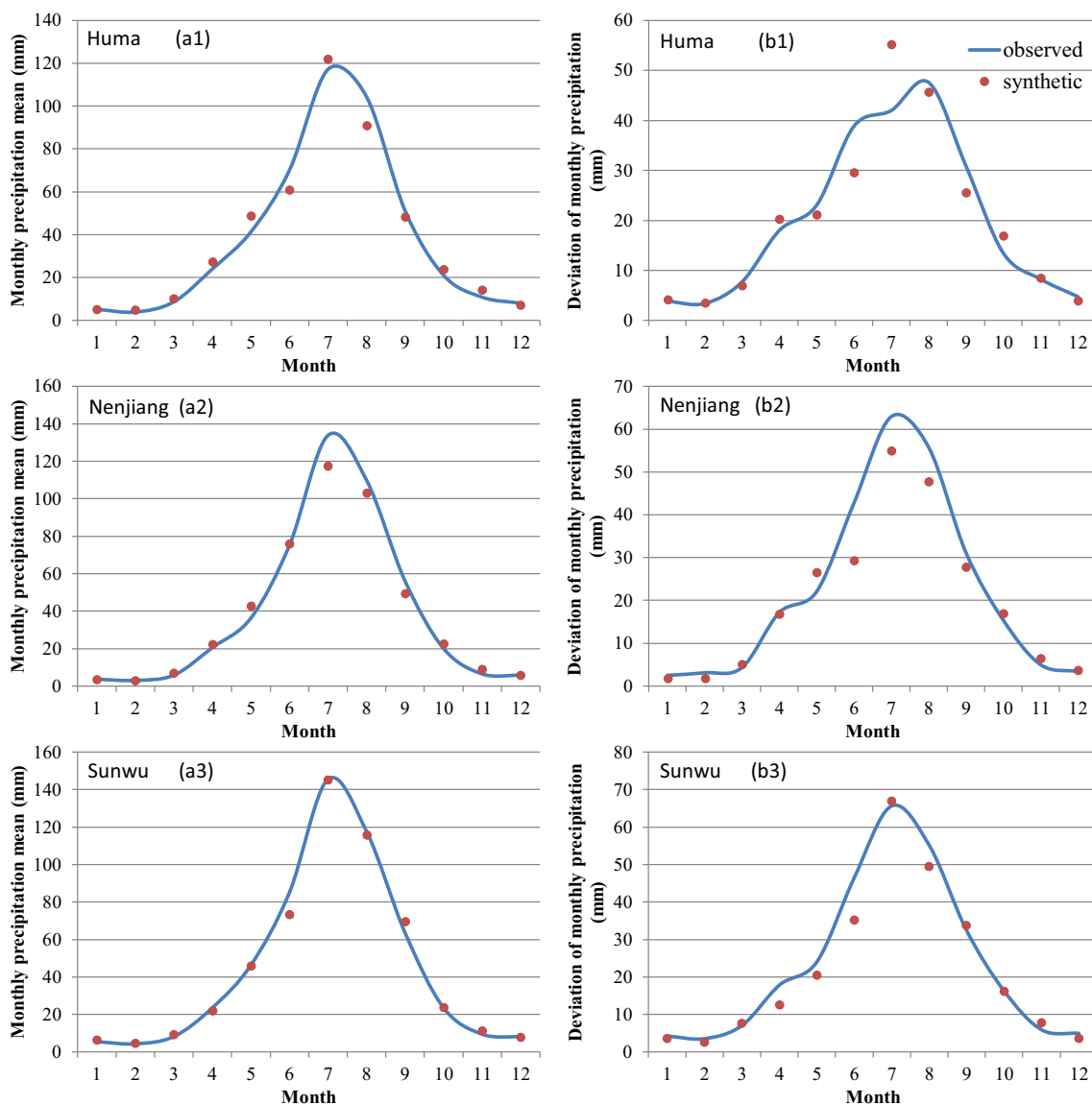


Fig. 2 Comparison of observed precipitation to simulated values from LARS-WG. Row a (**a1–a3**) represents the monthly mean, and row b (**b1–b3**) represents the standard deviation for each of three sites for the period of 1961 to 2010

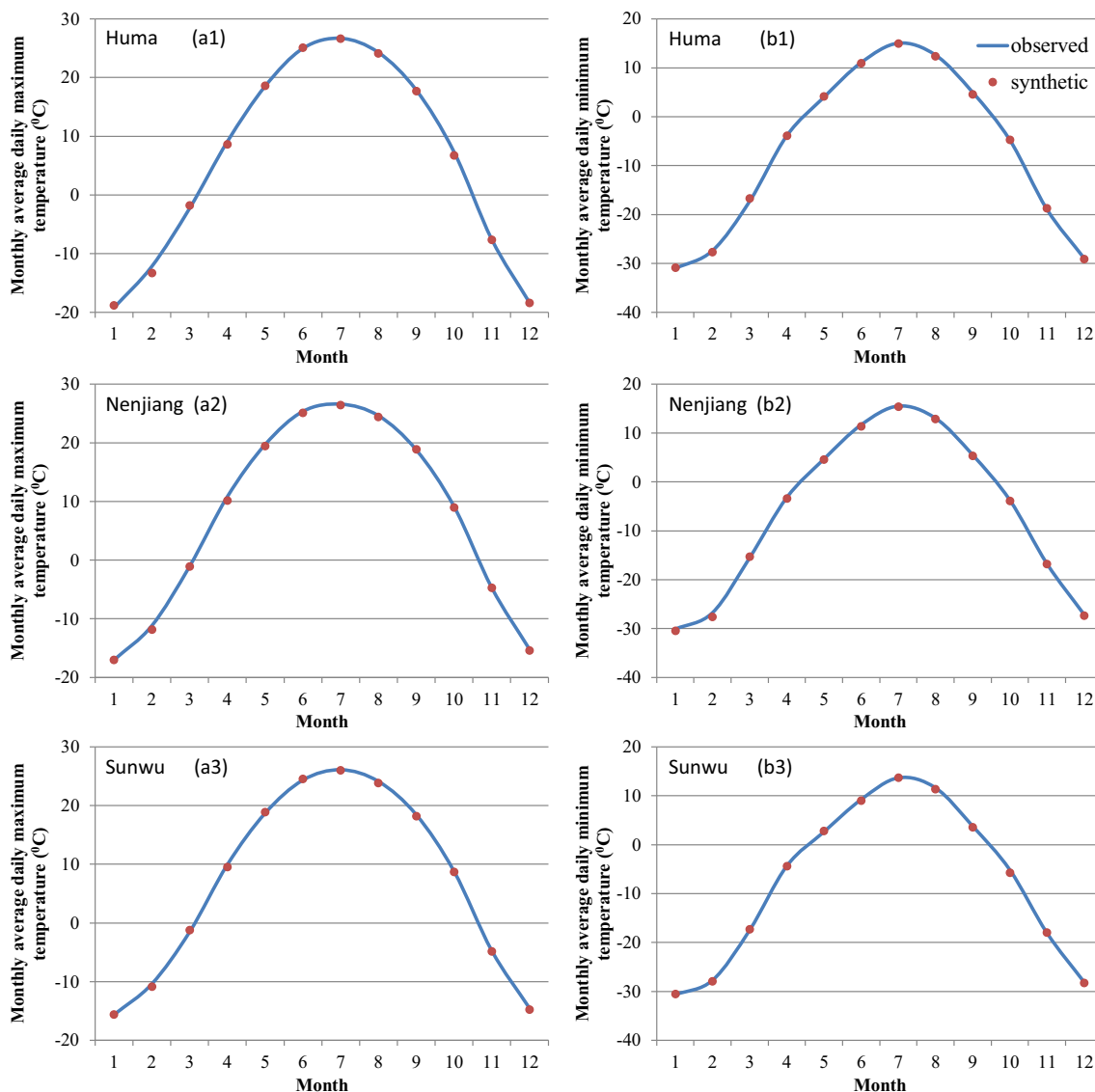


Fig. 3 Comparison of observed monthly temperatures to simulated values from LARS-WG. Row a (**a1–a3**) represents the daily maximum temperature, and row b (**b1–b3**) represents the daily minimum temperature, for each of three sites for the period of 1961 to 2010

estimation are reasonable. On the other hand, the simulated monthly mean of the daily maximum and minimum temperatures matches well with the observed values for all of the study sites in all months (Fig. 3). These model results indicate that the calibrated and validated LARS-WG model has great capacity for simulating weather data in northeastern China for all three stations as case sites in this study, based on which further estimations for future climates scenarios are possible.

3.2 Analysis of future climates scenarios

The changes in the monthly precipitation and mean daily Tmax and Tmin of the three studied stations for the periods 2046 to 2065 (2050s) and 2060 to 2079 (2070s) under three different RCP scenarios were estimated by the Python batch command based on 14 GCM outputs, the results of which are illustrated in

Fig. 4, 5, and 6. Common increasing trends in future precipitation and air temperature for all GCMs were observed, but there was no coherent variation among various GCMs, in accordance with other studies (Fenta Mekonnen and Disse 2018; Hussain et al. 2018). There will generally be more precipitation in the 2070s than 2050s. Scenarios with a higher radiative forcing level will lead to more precipitation in the 2070s. The relative increase in precipitation is mainly focused on winter months, while the absolute increase is mainly focused on summer months. For future air temperature analysis, both Tmax and Tmin will rise in the 2050s for all three scenarios. A higher air temperature could be expected under scenarios with higher radiative forcing level. For the RCP 8.5 scenario, an increasing trend is found in the 2070s, while the Tmax and Tmin will generally stay at the same level as the 2050s for RCP 2.6 and RCP 4.5. As seen in the monthly changing analysis, there will

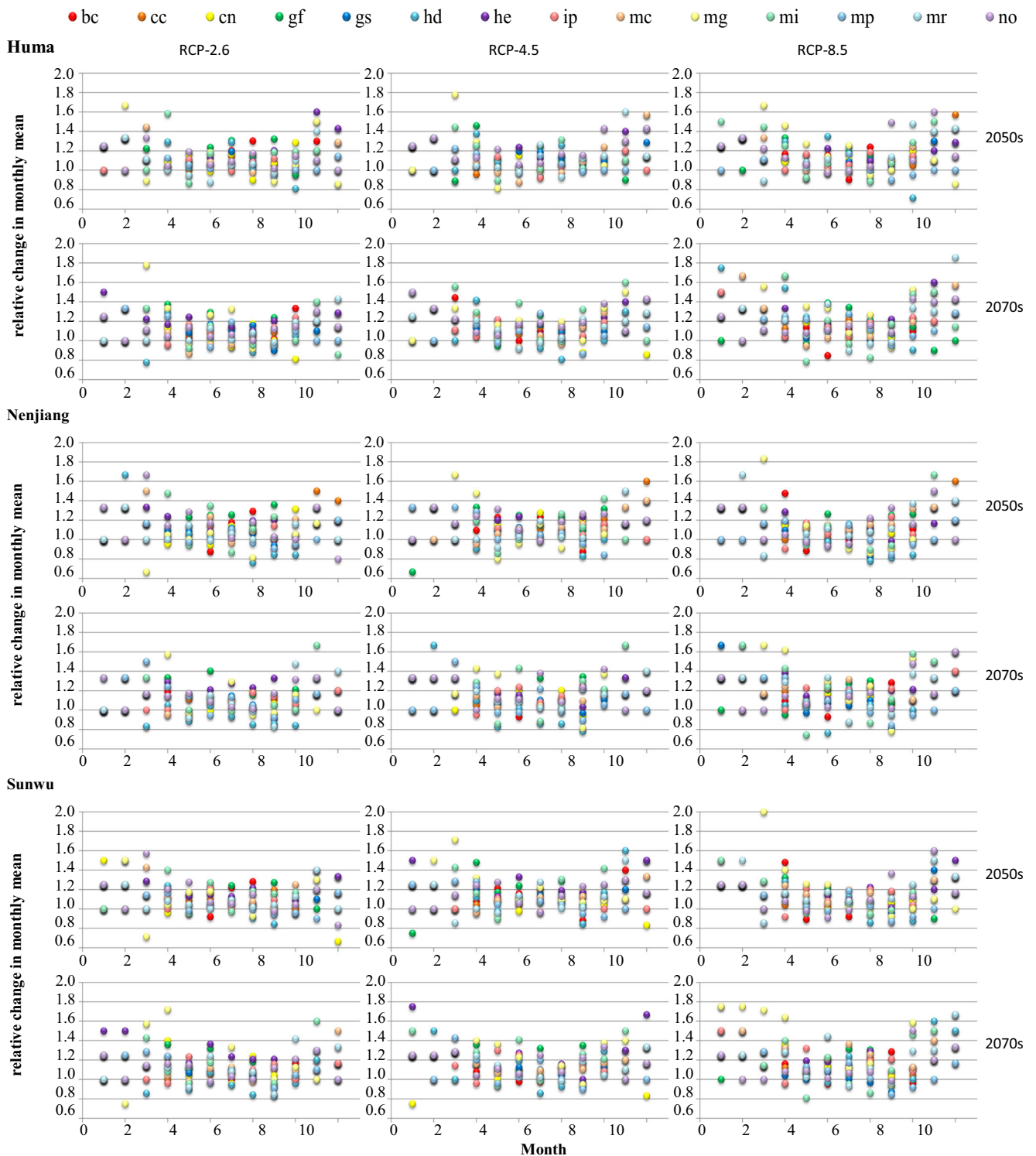


Fig. 4 Monthly changes in precipitation for each site in different RCP scenarios and future periods from various GCM outputs. bc BCC-CSM1-1, cc CCSM4, cn CNRM-CM5, gf GFDL-CM3, gs GISS-E2-R, hd

HadGEM2-AO, he HadGEM2-ES, ip IPSL-CM5A-LR, mc MIROC-ESM-CHEM, mg MIROC-ESM, mi MIROC5, mp MPI-ESM-LR, mr MRI-CGCM3, no NorESM1-M

be relatively intense increases in air temperature in winter months. These results can be used to update the model parameters of LARS-WG to generate synthetic daily weather data that represent different future periods under different RCP scenarios

from different GCMs. However, due to the great differences among the different outputs of GCMs, there is significant uncertainty in modeling future weather data based on one single GCM. To address this issue, ensemble means was achieved.

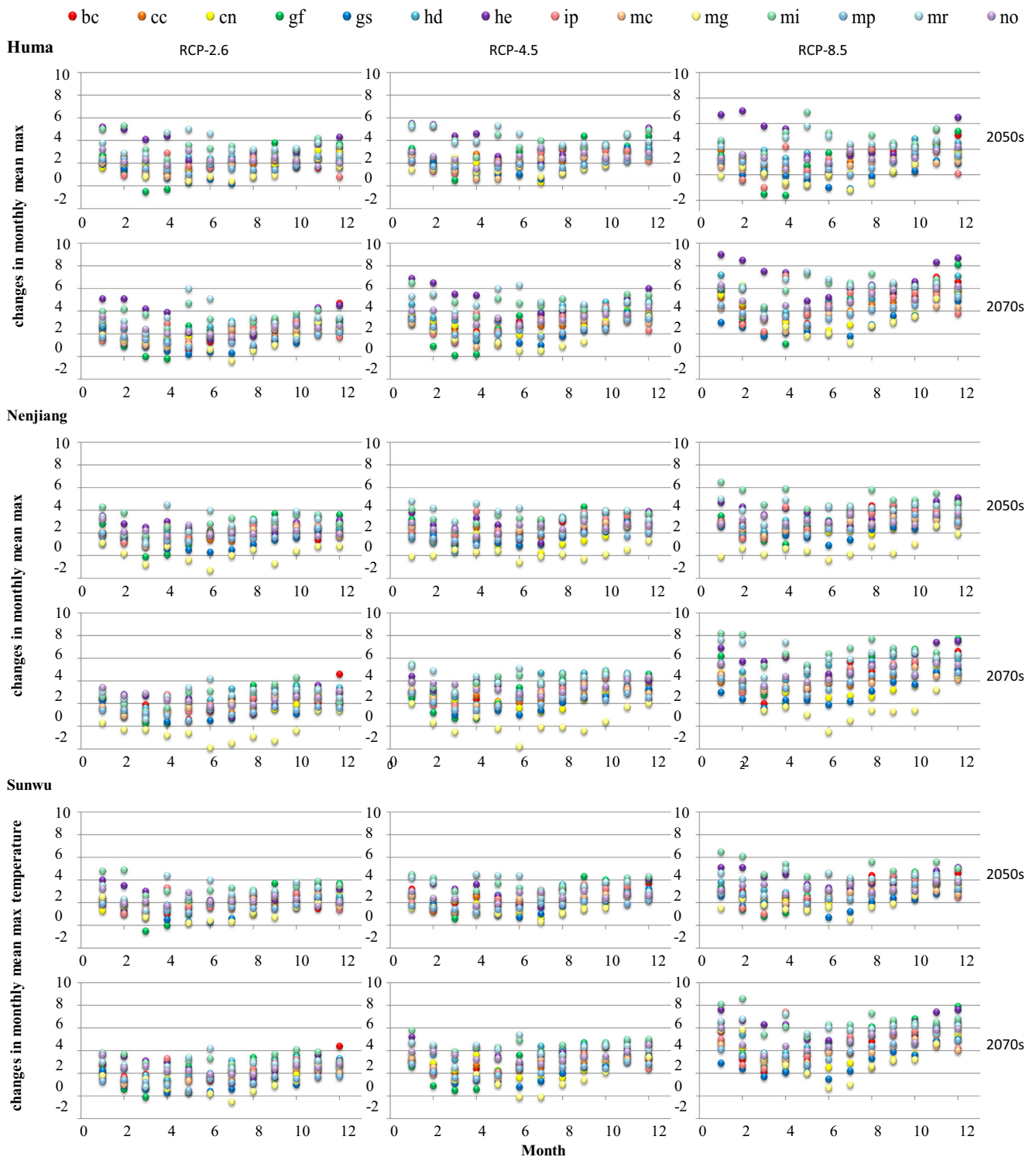


Fig. 5 Monthly changes in the maximum temperature for each site in different RCP scenarios and future periods from various GCM outputs. bc BCC-CSM1-1, cc CCSM4, cn CNRM-CM5, gf GFDL-CM3, gs

GISS-E2-R, hd HadGEM2-AO, he HadGEM2-ES, ip IPSL-CM5A-LR, mc MIROC-ESM-CHEM, mg MIROC-ESM, mi MIROC5, mp MPI-ESM-LR, mr MRI-CGCM3, no NorESM1-M

The average of all 14 GCM outputs was calculated and used together with the baseline values as the ensemble means to update the LARS-WG model parameters. For each site in this study, six scenario files were created that

represented relative changes in the monthly mean precipitation and absolute changes in the monthly Tmax and Tmin under three RCP scenarios and two future periods, respectively. These six scenario files were used in a

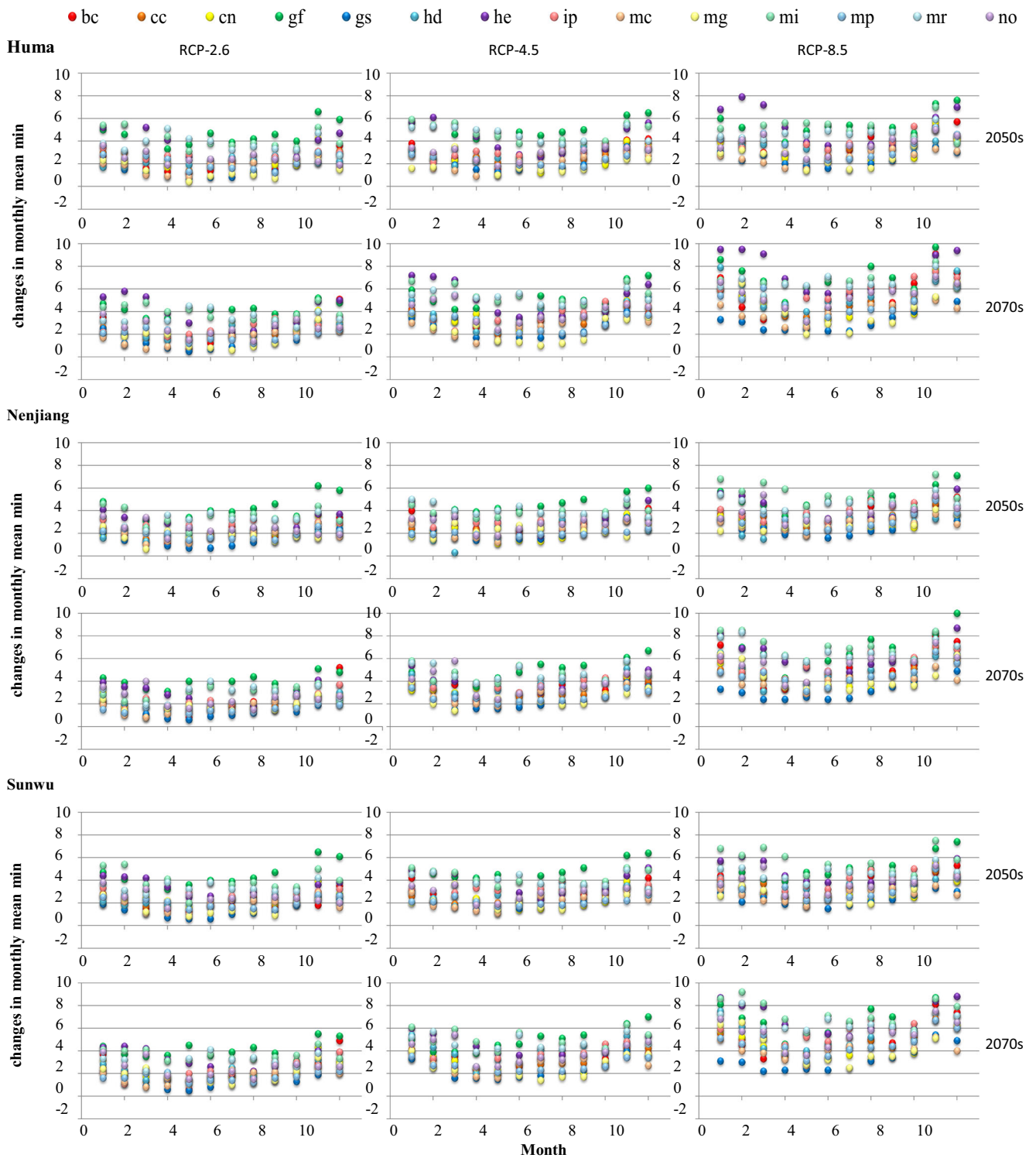


Fig. 6 Monthly changes of the minimum temperature for each site in different RCP scenarios and future periods from various GCMs' outputs. bc BCC-CSM1-1, cc CCSM4, cn CNRM-CM5, gf GFDL-

CM3, gs GISS-E2-R, hd HadGEM2-AO, he HadGEM2-ES, ip IPSL-CM5A-LR, mc MIROC-ESM-CHEM, mg MIROC-ESM, mi MIROC5, mp MPI-ESM-LR, mr MRI-CGCM3, no NorESM1-M

LARS-WG model to generate synthetic daily weather data for various predicted future statuses. Each group of LARS-WG implements was run for a long period of 50 years to consider extreme conditions (avoiding

uncertainty by neither missing nor magnifying the unusual weather influence), the results of which are plotted in Fig. 7. The length of the box represents the distance between the first quartile (25th percentiles) and third quartile

S0: Baseline level S1: RCP2.6 in 2050s S2: RCP2.6 in 2070s S3: RCP4.5 in 2050s S4: RCP4.5 in 2070s S5: RCP8.0 in 2050s S6: RCP8.0 in 2070s

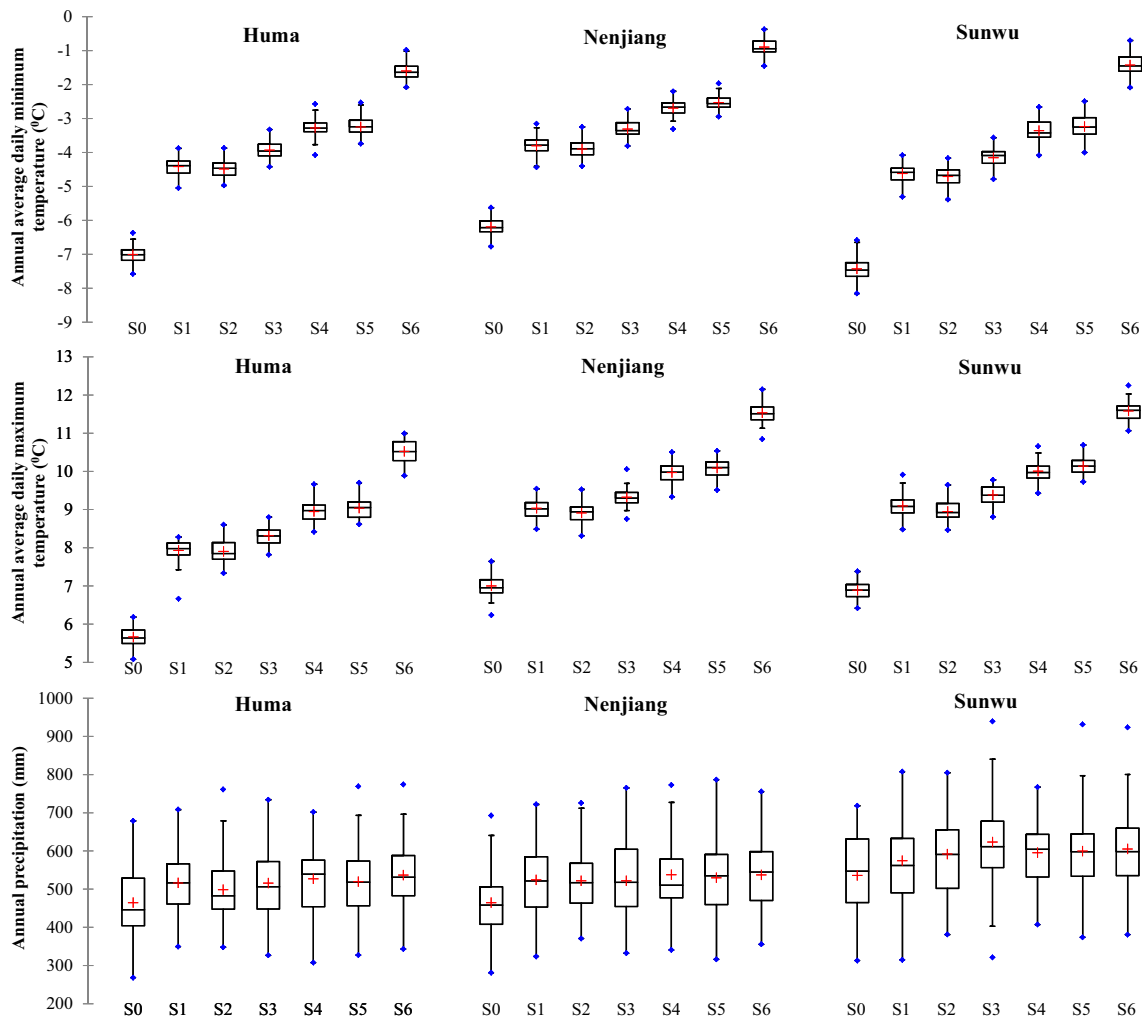


Fig. 7 Comparisons of the annual precipitation and maximum and minimum temperatures for each station under various RCP scenarios in different future periods compared with the baseline values. The upper and lower borders of the box represent the 25th percentiles and 75th

(75th percentiles), and the line and cross in the box interior represent the median and mean values in the group, respectively. The ends of the “whiskers” are the lower and upper limits, beyond which the values are considered anomalous. The minimum and maximum values of the group are shown into two solid points.

It is shown that there are common increases in air temperature and precipitation for most RCP scenarios in the future. In one hand, for T_{min} and T_{max} , a higher radiative forcing level would lead to a higher potential future air temperature. In the same future periods, RCP scenarios with higher radiative forcing levels would lead to greater increases in T_{min} and T_{max} . However, with the same radiative forcing level, the changes of T_{min} and T_{max} in different future periods would vary for different RCP scenarios; for RCP 2.6 scenarios, the T_{min} and T_{max} would increase in 2050s and then remain steady in the

percentiles, respectively, and line and cross in the box interior represent the median and mean values. The minimum and maximum values are shown as two solid points, while “whiskers” are lower and upper limits beyond which values are considered to be anomalous

2070s, while a similar continuous increasing trend can be found in all future periods for both RCP 4.5 and RCP 8.5 scenarios. For different weather sites, the Nenjiang station represented the greatest increases in T_{min} and the changes in Sunwu station would be the mildest. The changes in T_{max} in Nenjiang and Sunwu would be similar and both greater than that in Huma, which has the highest latitude of the three studied sites. In the other hand, we could learn that all the results indicated positive changes in precipitation in the future, but no significant correlation was found between the increases and radiative forcing levels. The changing trends under various RCP scenarios would differ for different sites in different future periods. For Huma and Nenjiang, there would be continuous increasing trends for precipitation under RCP 4.5 and RCP 8.5, but a decrease in precipitation in 2070s than 2050s under RCP 2.6. In addition, the

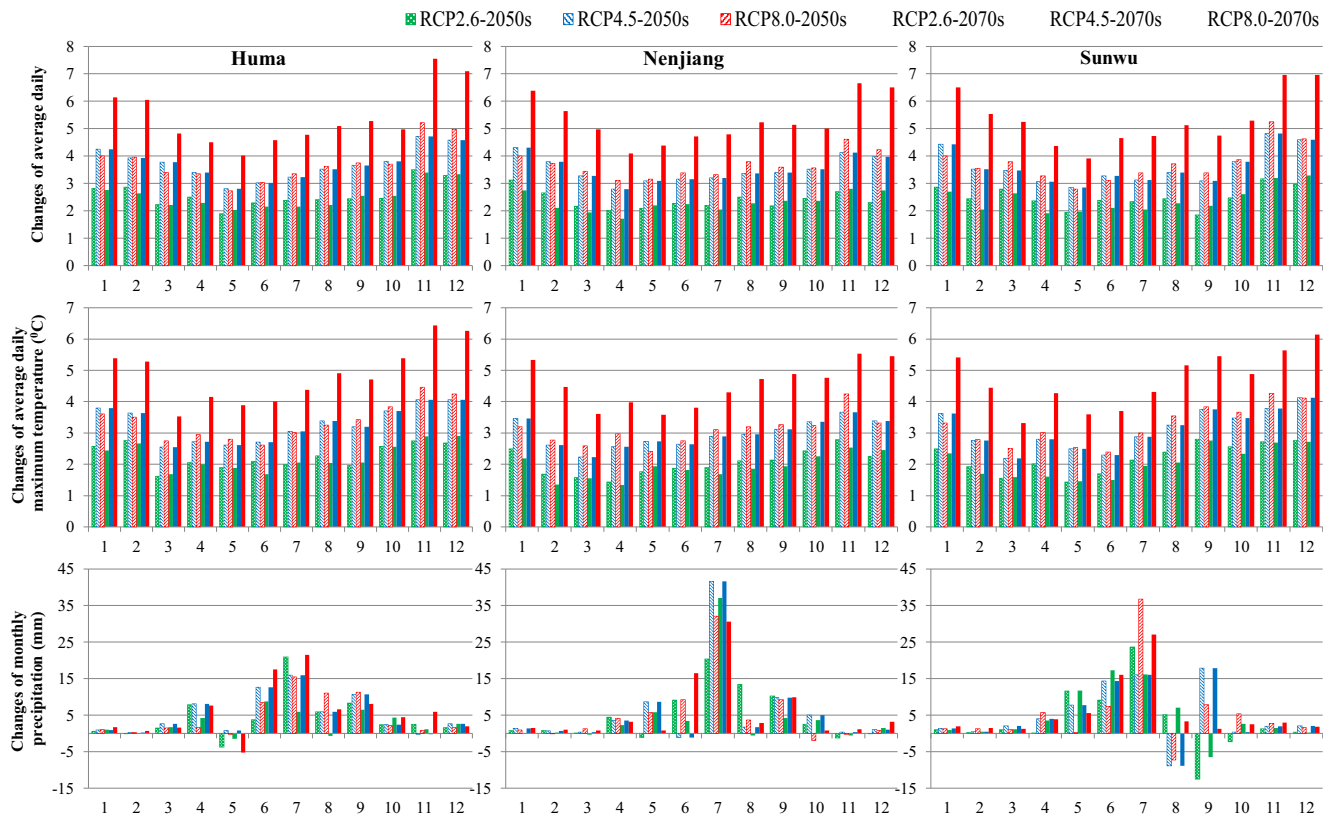


Fig. 8 Changes in the monthly precipitation and maximum and minimum temperatures in different months under various RCP scenarios in different future periods in three studied sites

highest increasing rates of precipitation would be observed in the 2070s under RCP 8.0 for both sites. For Sunwu, the highest increasing rate of precipitation would occur in the 2050s under RCP 4.5, but a decreasing trend could be found from 2050s to 2070s for this scenario. Continuous increasing trends were observed throughout the study periods under RCP 2.6 and RCP 8.5 in Sunwu.

In another view, the changes in monthly precipitation, Tmax and Tmin, are illustrated in Fig. 8. All three sites had similar changes in monthly precipitation, Tmax and Tmin. The precipitation showed increasing trends in most months, with several exceptions that occurred in Sunwu in August and September of 2050s. The increasing precipitation is mainly focused on hot summer months, with the greatest increases

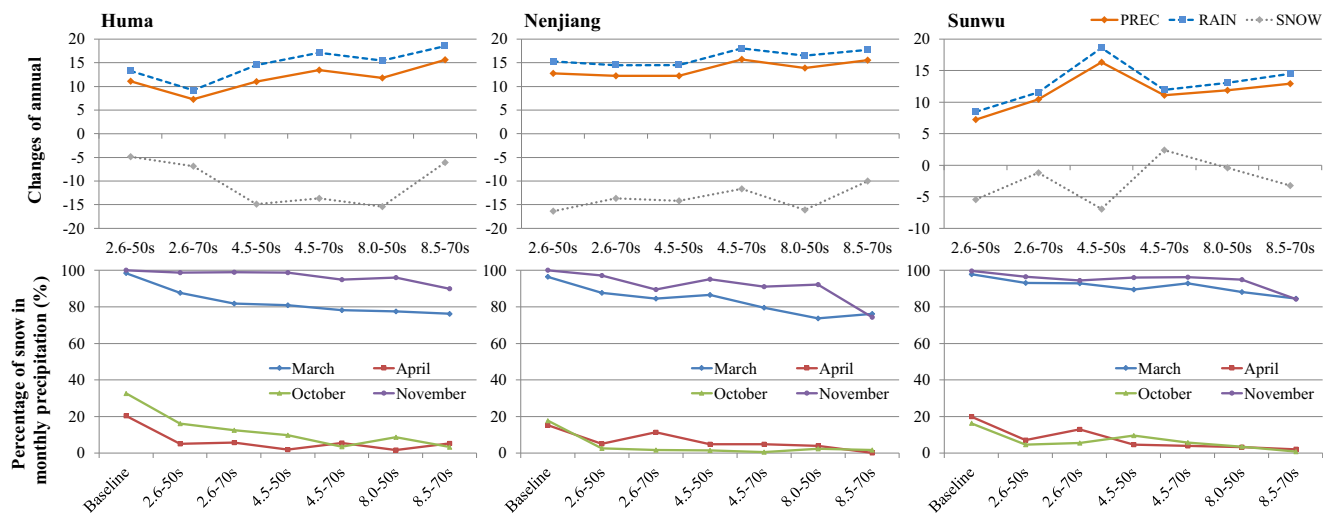


Fig. 9 Comparison of the changes of annual precipitation, annual rainfall, and annual snowfall, as well as the proportion of snowfall of total precipitation in early and late winter months, under various RCP scenarios in different future periods in three studied sites

in July. The increases of Tmax and Tmin in the future were coherent, and all months for the three sites in future periods will experience warmer weather based on model predictions. In addition, greater ratios of temperature increases are found in cold winter months. These results are consistent with IPCC reports and GCM outputs. From the above analysis, it was certain that warming and wetting would last in the future for the three sites, which could potentially disturb the regional environment. Warmer weather and a higher precipitation yield will have a significant influence on the form of precipitation, as discussed in Sect. 3.3.

3.3 Analysis of changes of future precipitation forms

On a mean annual scale, all three sites show increasing trends of annual rainfall and precipitation, while their snowfall generally decreases, as shown in Fig. 9. All three sites' snowfall will decrease relative to the baseline level, except Sunwu station under RCP 4.5 scenarios in the 2070s. There are similar trends for changes in annual precipitation and rainfall for the same site, which represent positive correlations with the radiative forcing level. In addition, the increasing rates of rainfall are higher than those of precipitation, possibly due to hotter weather conditions in the future.

Changes in snowfall could be considered to be the common effect of the changes of precipitation and temperature in the future. More precipitation is positive for an increase in snowfall, while higher temperatures are negative for future snowfall due to fewer snow events. The critical precipitation increases are focused in summer months from June to September (Fig. 8), indicating that more rain will occur in summer in the future, primarily resulting in an increasing trend in annual rainfall in the study area. More precipitation occurring in winter will bring more potential snowfall, but will be offset by precipitation form changes in early and late winter, considering future higher temperatures. In early winter, the number of days with Tmin in October and/or Tmax in November below the freezing point will be reduced, which means less snow but more rain in this period in the future. Similarly, there will be fewer freezing cold days for snow in late winter (March and April). These warmer weather conditions will result in smaller proportions of snowfall in monthly precipitation in these months (Fig. 9). However, benefiting from increases in total precipitation, particularly in the period from December to February when snow events are predominant, the snow cover in deep winter will increase and the annual snowfall will remain at a relatively steady level.

This snow-dominant situation should be of great concern. Less winter precipitation falling as snow and an earlier spring thaw will greatly impact the area surface conditions, with potential to cause severe impacts on agriculture and other related

aspects. Furthermore, with positive changes in snow cover accumulation due to the increasing precipitation in deep winter months, more and earlier snowmelt discharge will lead to a shift in the peak river runoff in early spring, which is critical for water resource management. In summary, the effects of further climate change in the cold area in northeastern China are significant and should be a subject of concern for local managers in decision-making.

4 Conclusions

The LARS-WG model was successfully applied in the northeastern China for modeling the daily precipitation, Tmin, and Tmax in a cold climate area. The long-term observed weather records from three case sites were well replicated by the calibrated model, based on which the future climate status from an ensemble of 14 GCMs' outputs in three CMIP5 scenario was downscaled to a series of daily precipitation, Tmin, and Tmax for the periods of 2050s and 2070s. The model results were compared and estimated, and the future weather features were discussed. The following three main conclusions can be drawn from the results of the present study:

1. The approach for using new outputs of GCMs under CMIP5 scenarios in LARS-WG model is valid, and the LARS-WG model can be used in cold areas to downscale daily precipitation, Tmax, and Tmin.
2. The downscaled model outputs based on different GCM predictions represent incoherent change trends that indicate significant uncertainties, and the ensemble approach based on multiple GCMs rather than a single GCM is recommended for future climate estimation.
3. There will be warmer and wetter conditions in the study area, with more rainfall but less snowfall, in the future. The increasing rainy events in the summer and earlier and heavier snowmelt in spring should be of great concern for local agricultural and water resource management.

Acknowledgments The authors acknowledge the developer of the LARS-WG model for access to software and license agreement. The data used for model application were provided by the Data Center for Resources and Environmental Sciences, Chinese Academy of Sciences (RESDC) (<http://www.resdc.cn>), and the China Meteorological Data Service Center (CMDSC) (<http://data.cma.cn>).

Funding information The study is financially supported by the innovation team training plan of the Tianjin Education Committee (TD13-5073), the National Natural Science Foundation of China (No. 41372373), the Opening Fund of Tianjin Key Laboratory of Water Resources and Environment (117-YF11700102), and the Science & Technology Development Fund of Tianjin Education Commission for Higher Education (2018KJ160).

Publisher's note Springer Nature remains neutral with regard to jurisdictional claims in published maps and institutional affiliations.

References

- Ahmadzadeh Araji H, Wayayok A, Massah Bavani A, Amiri E, Abdullah AF, Daneshian J, Teh CBS (2018) Impacts of climate change on soybean production under different treatments of field experiments considering the uncertainty of general circulation models. *Agric Water Manag* 205:63–71. <https://doi.org/10.1016/j.agwat.2018.04.023>
- Amin MZM, Islam T, Ishak AM (2014) Downscaling and projection of precipitation from general circulation model predictors in an equatorial climate region by the automated regression-based statistical method. *Theor Appl Climatol* 118:347–364. <https://doi.org/10.1007/s00704-013-1062-2>
- Bannayan M, Paymard P, Ashraf B (2016) Vulnerability of maize production under future climate change: possible adaptation strategies. *J Sci Food Agric* 96:4465–4474. <https://doi.org/10.1002/jsfa.7659>
- Chen H, Guo J, Zhang Z, Xu C-Y (2013) Prediction of temperature and precipitation in Sudan and South Sudan by using LARS-WG in future. *Theor Appl Climatol* 113:363–375. <https://doi.org/10.1007/s00704-012-0793-9>
- Conway D, van Garderen EA, Deryng D, Dorling S, Krueger T, Landman W, Lankford B, Lebek K, Osborn T, Ringler C, Thurlow J, Zhu T, Dalin C (2015) Climate and southern Africa's water-energy-food nexus. *Nat Clim Chang* 5:837–846. <https://doi.org/10.1038/nclimate2735>
- Dumont B, Basso B, Bodson B, Destain JP, Destain MF (2016) Assessing and modeling economic and environmental impact of wheat nitrogen management in Belgium. *Environ Model Softw* 79:184–196. <https://doi.org/10.1016/j.envsoft.2016.02.015>
- Fenta Mekonnen D, Disse M (2018) Analyzing the future climate change of Upper Blue Nile River basin using statistical downscaling techniques. *Hydrol Earth Syst Sci* 22:2391–2408. <https://doi.org/10.5194/hess-22-2391-2018>
- Fezzi C, Harwood AR, Lovett AA, Bateman IJ (2015) The environmental impact of climate change adaptation on land use and water quality. *Nat Clim Chang* 5:255–260. <https://doi.org/10.1038/nclimate2525>
- Gao X, Shi Y, Giorgi F (2011) A high resolution simulation of climate change over China. *Sci China Earth Sci* 54:462–472. <https://doi.org/10.1007/s11430-010-4035-7>
- Giorgi F, Lionello P (2008) Climate change projections for the Mediterranean region. *Glob Planet Chang* 63:90–104. <https://doi.org/10.1016/j.gloplacha.2007.09.005>
- Grafton RQ, Pittock J, Davis R, Williams J, Fu G, Warburton M, Udall B, McKenzie R, Yu X, Che N, Connell D, Jiang Q, Kompas T, Lynch A, Norris R, Possingham H, Quiggin J (2013) Global insights into water resources, climate change and governance. *Nat Clim Chang* 3:315–321. <https://doi.org/10.1038/nclimate1746>
- Hassan Z, Shamsudin S, Harun S (2014) Application of SDSM and LARS-WG for simulating and downscaling of rainfall and temperature. *Theor Appl Climatol* 116:243–257. <https://doi.org/10.1007/s00704-013-0951-8>
- Hijmans RJ, Cameron SE, Parra JL, Jones PG, Jarvis A (2005) Very high resolution interpolated climate surfaces for global land areas. *Int J Climatol* 25:1965–1978. <https://doi.org/10.1002/joc.1276>
- Hussain M, Yusof KW, Mustafa MRU, Mahmood R, Jia S (2018) Evaluation of CMIP5 models for projection of future precipitation change in Bornean tropical rainforests. *Theor Appl Climatol* 134:423–440. <https://doi.org/10.1007/s00704-017-2284-5>
- Kim HK, Parajuli PB, Filip To SD (2013) Assessing impacts of bioenergy crops and climate change on hydrometeorology in the Yazoo River Basin, Mississippi. *Agric For Meteorol* 169:61–73. <https://doi.org/10.1016/j.agrformet.2012.10.007>
- Kumar D, Arya DS, Murumkar AR, Rahman MM (2014) Impact of climate change on rainfall in northwestern Bangladesh using multi-GCM ensembles. *Int J Climatol* 34:1395–1404. <https://doi.org/10.1002/joc.3770>
- Ma C, Pan S, Wang G, Liao Y, Xu Y-P (2016) Changes in precipitation and temperature in Xiangjiang River Basin. *China Theor Applied Climatol* 123:859–871. <https://doi.org/10.1007/s00704-015-1386-1>
- Mahat V, Anderson A (2013) Impacts of climate and catastrophic forest changes on streamflow and water balance in a mountainous headwater stream in southern Alberta. *Hydrol Earth Syst Sci* 17:4941–4956. <https://doi.org/10.5194/hess-17-4941-2013>
- McNutt M (2013) Climate change impacts. *Science* 341:435–435. <https://doi.org/10.1126/science.1243256>
- Naderi M, Raeisi E (2016) Climate change in a region with altitude differences and with precipitation from various sources, South-Central Iran. *Theor Appl Climatol* 124:529–540. <https://doi.org/10.1007/s00704-015-1433-y>
- Pervez MS, Henebry GM (2014) Projections of the Ganges–Brahmaputra precipitation—downscaled from GCM predictors. *J Hydrol* 517:120–134. <https://doi.org/10.1016/j.jhydrol.2014.05.016>
- Qin XS, Lu Y (2014) Study of climate change impact on flood frequencies: a combined weather generator and hydrological modeling approach. *J Hydrometeorol* 15:1205–1219. <https://doi.org/10.1175/jhm-d-13-0126.1>
- Reddy KS, Kumar M, Maruthi V, Umesh B, Vijayalaxmi RC (2014) Climate change analysis in southern Telangana region, Andhra Pradesh using LARS-WG model. *Curr Sci* 107:54–62
- Sanchez E, Gallardo C, Gaertner MA, Arribas A, Castro M (2004) Future climate extreme events in the Mediterranean simulated by a regional climate model: a first approach. *Glob Planet Chang* 44:163–180. <https://doi.org/10.1016/j.gloplacha.2004.06.010>
- Sarkar J, Chicholikar JR, Rathore LS (2015) Predicting future changes in temperature and precipitation in arid climate of Kutch, Gujarat: analyses based on LARS-WG model. *Curr Sci* 109:2084–2093
- Semenov MA, Barrow EM (1997) Use of a stochastic weather generator in the development of climate change scenarios. *Clim Chang* 35:397–414. <https://doi.org/10.1023/a:1005342632279>
- Semenov MA, Stratonovitch P (2015) Adapting wheat ideotypes for climate change: accounting for uncertainties in CMIP5 climate projections. *Clim Res* 65:123–139
- Solow AR (2015) Extreme weather, made by us? *Science* 349:1444–1445. <https://doi.org/10.1126/science.aad2132>
- Stevens B, Giorgetta M, Esch M, Mauritsen T, Crueger T, Rast S, Salzmann M, Schmidt H, Bader J, Block K, Brokopf R, Fast I, Kinne S, Kornblueh L, Lohmann U, Pincus R, Reichler T, Roeckner E (2013) Atmospheric component of the MPI-M earth system model: ECHAM6. *J Adv Model Earth Syst* 5:146–172. <https://doi.org/10.1002/jame.20015>
- Tripathi S, Srinivas VV, Nanjundiah RS (2006) Downscaling of precipitation for climate change scenarios: a support vector machine approach. *J Hydrol* 330:621–640. <https://doi.org/10.1016/j.jhydrol.2006.04.030>
- Vallam P, Qin XS (2018) Projecting future precipitation and temperature at sites with diverse climate through multiple statistical downscaling schemes. *Theor Appl Climatol* 134:669–688. <https://doi.org/10.1007/s00704-017-2299-y>
- Wilby RL, Dawson CW, Barrow EM (2002) SDSM—a decision support tool for the assessment of regional climate change impacts. *Environ Model Softw* 17:147–159
- Zarghami M, Abdi A, Babaeian I, Hassanzadeh Y, Kanani R (2011) Impacts of climate change on runoffs in East Azerbaijan, Iran. *Glob Planet Chang* 78:137–146. <https://doi.org/10.1016/j.gloplacha.2011.06.003>
- Zhang XC (2005) Spatial downscaling of global climate model output for site-specific assessment of crop production and soil erosion. *Agric For Meteorol* 135:215–229. <https://doi.org/10.1016/j.agrformet.2005.11.016>